

A Second-Order Optical Butterworth Fabry-Pérot Filter

Zeyang Li,^{1, a)} Abhishek V. Karve,^{1, a)} Xin Wei,^{1, a)} and Jonathan Simon^{1, 2}

¹⁾*Department of Applied Physics, Stanford University, Stanford, CA*

²⁾*Department of Physics, Stanford University, Stanford, CA*

(*Electronic mail: jonsimon@stanford.edu)

Filters with flat-top pass-bands are a key enabling technology for signal processing. From communication to sensing, the ability to choose a pass *band*, rather than a single pass *frequency*, while still efficiently suppressing backgrounds at other frequencies, is a critical capability for ensuring both detection sensitivity and power efficiency. Efficient transmission of a single frequency can be achieved by a single-pole resonator—which in optics is a Fabry-Pérot cavity offering linewidths from kHz to GHz and beyond. Coupling multiple resonators allows for the construction of flat-top multi-pole filters. These, although straightforward from RF to THz where resonators are macroscopic and tunable, are more difficult to control in the optical band and typically realized with dielectric stacks, whose passband widths exceed 100 GHz. Here, we bridge the gap to narrower bandwidth flat-top filters by proposing and implementing a second-order Butterworth-type optical filter in a single two-mirror Fabry-Pérot cavity, by coupling the two polarization modes. We demonstrate a pass-band width of 2.68(1) GHz, a maximum stopband suppression of 43 dB, and a passband insertion loss of 2.2(1) dB, with out-of-band power suppression falling as the fourth power of detuning. This approach is viable down to much narrower filters, and has the potential to improve high-frequency phase noise performance of lasers, enhance the sensitivity of LIDARs, and provide higher quality narrowband filtering, for example, for Raman spectroscopy.

I. INTRODUCTION

Band-pass filters (with a flat passband) are a standard tool in modern microwave and RF engineering to separate a desired signal from undesirable components at other frequencies. In the optical regime, dielectric-stack filters can achieve similar effects^{1–3}, but with a slope’s width at the 0.1 nm (~ 50 GHz at 780 nm) level. Such filters are not ideal for certain precise applications, including many in atomic physics experiments, where the required passband is typically no more than a few GHz wide^{4–8}.

On the other hand, optical cavities can serve as narrow first-order filters⁹, efficiently transmitting a single frequency before *immediately* suppressing signals off of the transmission resonance, with a field-suppression that scales inversely with detuning, with bandwidths down to kHz^{10,11}. Fabry-Pérot filters, for example, are commonly employed for frequency-selection and stabilization in lasers^{12–15}, Raman spectroscopy^{16–19}, sum frequency generation spectroscopy^{20,21}, double resonance 2D-IR spectroscopy^{22,23}, and pulse-laser shaping^{16,24}. Such a cavity, however, is a first-order filter with a Lorentzian shape, characterized by the slow $1/\delta^2$ roll-off with the laser detuning from the filter center (δ) in the wings without a flat transmission region at the top. As an example, distributed Bragg reflector (DBR) lasers have been shown to stabilize to subkilohertz linewidths by using long external cavities²⁵. This approach would benefit from a filter that has a flat-top transmission with faster roll-off in its wings.

High-order—such as Butterworth-type—filters²⁶, can achieve a flatter transmission band and a faster roll-off within the rejection band. Efforts towards flat-top optical filters have

been primarily aimed at wideband nano- / micro-photonic^{27,28} devices, where the small size and relatively low finesse of the filters combine to ensure that the filter passbands never reach the GHz-to-sub GHz regime. Active gain media have been proposed as an ingredient of Parity-Time (PT)-symmetric flat-top filters²⁹, but the fine-tuned nature of the device makes it generally difficult to realize, and its added noise makes it fundamentally incompatible with filtering of single photon signals.

Realizing such narrowband, high-order optical filters should be possible by cascading Fabry Pérot resonators^{30,31}, and while coupled macroscopic systems have been controlled³², simultaneously locking multiple resonators is technically challenging. In this letter, we report our demonstration of a compact & robust free-space second-order Butterworth optical filter where the two employed resonator modes are *geometrically frequency locked to one another*, achieved by coupling the two polarization modes of a single two-mirror cavity.

II. SECOND ORDER FILTERS IN TERMS OF COUPLED RESONATORS

A second-order filter with a full width at half maximum (FWHM) of κ —can also be thought of as the power loss rate—can be implemented in transmission through two cascaded cavities, each with a FWHM (due to their non-shared mirrors) of $\kappa/\sqrt{2}$, and a coupling Rabi frequency of $\kappa/\sqrt{2}$ as well^{33–35}, as defined in the inset in Fig. 1. This precise matching between the input/output rate and the resonator coupling strength can be thought of as a kind of optical impedance matching that ensures *both* a flat-topped spectral response *and* 100% transmission on resonance.

This device acts as a second-order filter because the light must pass through *two* cavities, in sequence, to be transmitted; the top of the filter is flattened by mode splitting induced

^{a)}These authors contributed equally.

by the coupling between the cavities. Viewed another way: the mode coupling generates two “dressed” modes, each a superposition of excitations in both cavities. The transmitted fields from the two modes interfere constructively *between* the modes, leading to a flat-topped transmission. The fields interfere destructively *outside* of the two modes, leading to the second-order field suppression.

This approach is fundamentally different from having a cavity followed by an optical isolator followed by a cavity. Such an object would act as two first-order filter and have a transmission spectrum of a Lorentzian squared. Such a response also provides the faster roll-off in the wings but does not provide the desired flat-top transmission. Allowing for the back coupling of the second cavity into the first cavity is what gives the flat-top *and* the faster roll-off in the wings.

The non-Hermitian Hamiltonian that describes the coupled-cavity system that yields an ideal second-order filter is³⁴:

$$\hat{H}_{2\text{nd}} = \omega_c \mathbb{I}_2 (\hat{a}^\dagger \hat{a} + \hat{b}^\dagger \hat{b}) + \frac{1}{2} \left(\frac{\kappa}{\sqrt{2}} \right) (\hat{a}^\dagger \hat{b}^\dagger) \begin{pmatrix} i & 1 \\ 1 & i \end{pmatrix} \begin{pmatrix} \hat{a} \\ \hat{b} \end{pmatrix}, \quad (1)$$

where \hat{a} and \hat{b} are annihilation operators of the two cavity modes, \mathbb{I}_2 is the 2×2 identity, ω_c is the center resonance frequency of the filter, and κ is the full width at half maximum of the filter as defined in Fig. 1. Since the Hamiltonian is linear, we will omit the creation and annihilation operators and use the 2×2 matrix to represent the Hamiltonian, with the bases $|1\rangle \equiv \hat{a}^\dagger |\text{vac}\rangle$ and $|2\rangle \equiv \hat{b}^\dagger |\text{vac}\rangle$ where $|\text{vac}\rangle$ is the vacuum state of both cavity modes. By using the non-Hermitian perturbation theory^{32,36,37}, the ratio of the output power from the second cavity to the input power of the first cavity with laser frequency ω_l is given by

$$T = \left| \frac{\kappa}{\sqrt{2}} \left\langle 1 \left| \frac{1}{\hat{H}_{2\text{nd}} - \omega_l \mathbb{I}_2} \right| 2 \right\rangle \right|^2 = \frac{1}{1 + (2\delta/\kappa)^4}, \quad (2)$$

where $\delta \equiv \omega_l - \omega_c$ is the driving detuning from the cavity. The transmission can also be derived from a scattering matrix approach³², as elaborated in Appendix A.

The shape exhibits an ideal second-order flat-top and a fast-decaying transfer function with a FWHM of κ . The Hamiltonian can be diagonalized into the form,

$$\hat{H}_{2\text{nd},d} = \omega_c \mathbb{I}_2 + \frac{1}{2} \left(\frac{\kappa}{\sqrt{2}} \right) \begin{pmatrix} i+1 & 0 \\ 0 & i-1 \end{pmatrix}, \quad (3)$$

the eigenmodes of which are split by $\kappa/\sqrt{2}$.

A. Polarization-Basis Coupled Cavity

There are various ways to implement the coupled cavities; the most direct is to employ three dielectric mirrors in sequence, akin to prior mode-conversion work³². Such an approach necessitates precise stabilization of two *separate* resonator lengths, fine-tuned control of the transmissive coupling between the two cavities, and precise mode-matching.

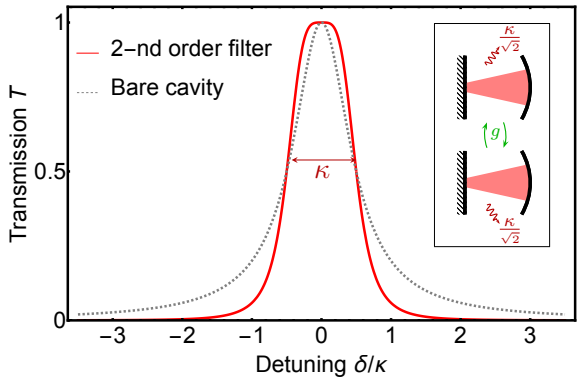


FIG. 1. Theoretical spectra of the second-order filter. The transfer function T (red solid line) of the second-order coupled cavity system is shown as a function of detuning between the frequency of the input light and the central resonant frequency of the system. This is compared with the bare cavity Lorentzian transmission (gray dashed line). The two transfer function spectra share the same peak transmission and a full width at half maximum (FWHM) of κ , while the second-order filter exhibits a flatter top and faster roll-off in its wings. The inset shows how such a filter can be thought of as two coupled single-ended cavity resonators, each with a power loss rate of $\kappa/\sqrt{2}$. The coupling Rabi frequency between the two cavity modes is defined as g . To achieve a flat-top transmission spectrum, the coupling needs to be tuned to $g = \kappa/\sqrt{2}$, as explained further in the main text.

Here, we explore a simpler approach, leveraging the two polarization modes of a *single* two-mirror Fabry-Pérot cavity, with birefringence-induced coupling between the modes. The coupling needed for the Hamiltonian in (3), can—when the two modes under consideration are orthogonal polarization states—arise *directly* from birefringence. Such a coupling can be turned on and controlled via an intra-cavity birefringent optic. This single-cavity implementation benefits us by automatically matching the loss rates of the two cavity modes. This approach provides a system with fewer degrees of freedom that must be actively stabilized, and continuous control of mode coupling through the tunable birefringence.

We explore two approaches to generate a small tunable birefringence in a low-loss (and thus cavity-compatible) optic: The first is to use a high (n th-) order half-wave plate (HWP). At normal incidence, the double-pass birefringence is exactly 2π and thus the modes are unsplit. To induce a controlled mode-coupling, we *tilt* the intra-cavity HWP about the z -axis for a non-normal incidence angle θ —deviating from an ideal HWP, as shown in Fig. 2(a). We then *rotate* the waveplate such that its extraordinary axis is at an angle ϕ from the z -axis. The ordinary and extraordinary axes of the HWP can be decomposed into their Cartesian components,

$$\begin{aligned} \hat{e}_o &= \sin \phi \hat{e}_z - \cos \phi (\cos \theta \hat{e}_y - \sin \theta \hat{e}_x), \\ \hat{e}_e &= \cos \phi \hat{e}_z + \sin \phi (\cos \theta \hat{e}_y - \sin \theta \hat{e}_x). \end{aligned}$$

For the cavity light in polarization $\hat{e}_\alpha = \cos \alpha \hat{e}_z + \sin \alpha \hat{e}_y$,

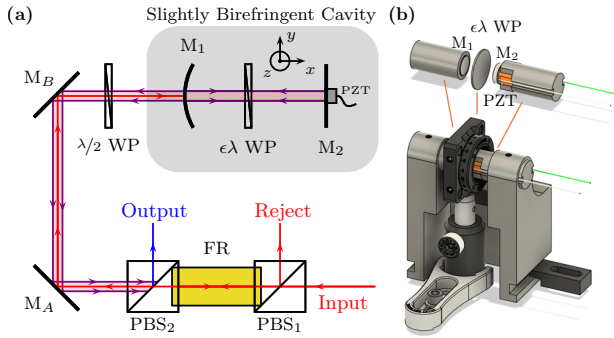


FIG. 2. Experimental setup of the second-order filter. (a) Polarization basis coupled cavity scheme for the second-order optical filter. The polarization of the input light (red) is aligned such that it transmits through the polarizing beam splitter (PBS₁), a Faraday Rotator (FR), and PBS₂. The two PBSs and the FR are part of Thorlab's IO-3-780-HP optical isolator. The polarization is then matched to the cavity polarization mode by a $\lambda/2$ wave plate (WP). It is then incident on a curved, partially reflective mirror M₁. The coupling of the polarization modes is achieved through an intra-cavity birefringent optic that acts like a $\epsilon\lambda$ WP—two implementations of such an optic are discussed in the main text. The cavity length is stabilized by the piezoelectric stack (PZT) on the high-reflectivity end mirror (M₂), by locking on the slope to a different wavelength (5 nm away), which is separated from the output by a conventional dielectric-stack filter. The cavity is single-ended, and all light goes back through M₁. The output (purple, shown as a bigger beam for convenience) carries a polarization superposition of the input light and its orthogonal component. The orthogonal polarization (blue) is reflected by PBS₂ and is the ‘output’ light of the filter. The input polarization component (red) gets reflected by PBS₁ and is the ‘rejected’ light of the filter. (b) CNC-machined monolithic mount of the cavity structure to suppress acoustic noise. The zoomed-in view shows the mirrors and the birefringent optic as they relate to the schematic in (a).

the round-trip shift is

$$\begin{aligned}\Delta\Phi(\alpha) &= \frac{2(m+1)\pi}{\cos\theta} |\hat{e}_\alpha \cdot \hat{e}_e| \\ &= \frac{2(m+1)\pi}{\cos\theta} (\sin\phi \cos\theta \sin\alpha + \cos\phi \cos\alpha),\end{aligned}$$

which corresponds to the two eigenmodes at $\alpha = \arctan(\cos\theta \tan\phi)$, $\arctan(\cos\theta \tan\phi) + \pi/2$ with a frequency splitting of,

$$\frac{2g}{2\pi \times \text{FSR}} = \sqrt{1 - \sin^2\theta \sin^2\phi} \times (m+1) \frac{1 - \cos\theta}{\cos\theta}, \quad (4)$$

where FSR stands for the free spectral range. This indicates that the coupling strength g is coarsely tuned by θ and finely-tuned by ϕ , which also guarantees a wide tuning range of g , from zero to $2\pi \times \text{FSR}$.

Our second approach leverages the fact that, in practice, the required birefringence is quite low. We introduce stress birefringence into the cavity by applying a uniaxial force to an otherwise non-birefringent thin glass plate. This approach avoids having to tilt any intra-cavity optics and lowers the minimum cavity length—up to considerations of the radius of

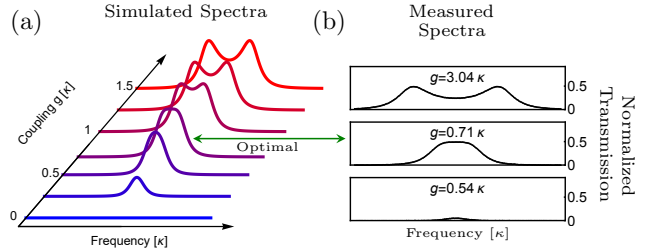


FIG. 3. Controlling the birefringence splitting. (a) The simulated filtered spectrum as a function of the induced birefringent coupling strength g . We show a full density plot of the simulated spectra in Appendix B. (b) Experimentally measured spectra of the second-order filter. The green arrow indicates the optimal filter performance in the simulated and measured spectra. Coupling strength g , obtained from fitting the transmission to (5), is shown for each spectrum. The desired flat-transmission performance is achieved at the optimal coupling value of $g = \kappa/\sqrt{2} \approx 0.71\kappa$ where κ is the linewidth of the coupled cavity system.

curvature of the mirrors—to the thickness of the glass plate (~ 1 mm), enabling larger resonator free-spectral ranges up to ~ 300 GHz. Data in Fig. 4 were collected using this approach.

B. Filter Transmission Spectra

The Hamiltonian under a birefringence splitting of g is

$$\hat{H}_{\text{birefringence}}(g) = \omega_c \mathbb{I}_2 + \frac{1}{2} \begin{pmatrix} i\frac{\kappa}{\sqrt{2}} & g \\ g & i\frac{\kappa}{\sqrt{2}} \end{pmatrix},$$

and the filtered spectrum, i.e., the transmission through the other mode, is given by

$$\begin{aligned}T(g) &= \left| \frac{\kappa}{\sqrt{2}} \left\langle 1 \middle| \frac{1}{\hat{H}_{\text{birefringence}}(g) - \omega_l \mathbb{I}_2} \middle| 2 \right\rangle \right|^2 \\ &= \frac{8g^2\kappa^2}{4g^4 + 4g^2(\kappa^2 - 8\delta^2) + (\kappa^2 + 8\delta^2)^2},\end{aligned} \quad (5)$$

as shown in Fig. 3(a). By changing θ, ϕ of the m -th order HWP or by changing the stress on the glass plate, we can operate at different values of g . As seen in Fig. 3(b), we obtained several filtered light spectra which exhibit the under-coupled, critically-coupled, and over-coupled regimes. The critically coupled point sits at $g = \sqrt{2}(\kappa/2)$ where we regain our Butterworth filter form of (1) and the transmission follows the characteristic flat-top transmission and fast decay in the wings of (2). The fundamental allowed transmission at critical coupling is 100%. The loss factors in our experiment are further discussed in section III.

III. EXPERIMENTAL PERFORMANCE

With the mount shown in Fig. 2(b), we can vary the cavity length by orders of magnitude. The curved mirror and

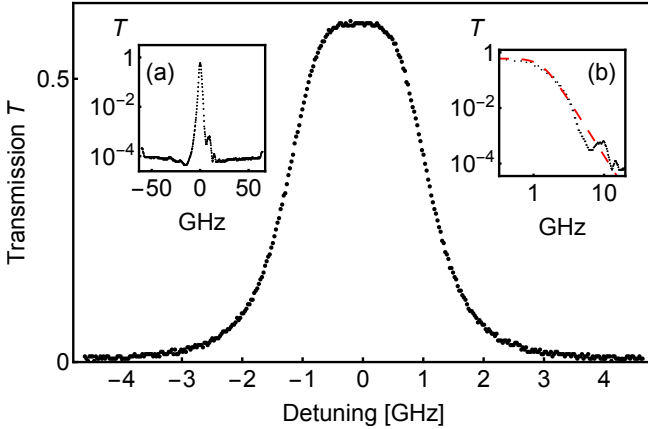


FIG. 4. Filtered transmission spectrum of the second-order filter under the optimal coupling with an FSR of 125 GHz, a FWHM of 2.68(1) GHz, and an insertion loss of 2.2(1) dB. Transmission is normalized to input power. Inset (a): the log-linear scale plot exhibits a ~ 40 dB suppression of background at $FSR/2$ away from center. Inset (b): the log-log scale plot showing the fast fall-off (black points) along with the theoretically predicted fall-off (red dashed line) of a second-order filter.

the thickness of the waveplate limit the maximum FSR to ~ 120 GHz, while the FSR can be arbitrarily small up to the cavity stability limits imposed by the mirror curvature. For our demonstration, we assemble a second-order filter with a width of $\kappa = 2\pi \times 2.68(1)$ GHz (finesse = 45). For this filter, the maximum possible suppression is $(2 \times \text{finesse}/\pi)^4 \sim 6.7 \times 10^5 = 58$ dB. As shown in Fig. 4, we have obtained an ideal second-order filter until imperfect mode-matching causes the higher-order transverse mode to appear at around 10 GHz detuning.

The filter has an insertion loss of 2.2(1) dB, which is set by the combination of multiple loss factors, including the fiber coupling, mode matching, isolator transmission, and dielectric loss from the cavity mirror. These factors are technical limitations and can be individually and simultaneously improved upon in future iterations of this filter. The fundamental limit on the peak transmission is 100%.

The maximum suppression is measured to be 43 dB, bounded by the rejection limit of the IO-3-780-HP isolator rather than the resonator finesse. The maximum suppression is seen around 15 GHz detuning (as seen in Fig. 4 inset (a)) due to the combined effects of interference between different spatial modes and the insufficient polarization extinction ratio of the PBS within the isolator. In the next generation of filters, we plan to use a 50dB extinction-ratio PBS (UFPBS10A) to determine the exact scaling and better distinguish the two effects.

The behavior near resonance is well described as an ideal second-order filter, with the first deviation occurring around 3 GHz (as seen in Fig. 4 inset (b)), resulting from imperfect mode matching that excites higher-order transverse modes. Precise alignment allowed us to completely suppress coupling to the TEM_{10} and TEM_{01} modes, but suppressing higher-order modes would require further beam *shaping* and, in practice,

allow transmission at the 6×10^{-4} level at 10 GHz detuning.

IV. OUTLOOK AND APPLICATIONS

We have demonstrated a minimal, robust, narrow-band high-order optical filter. We have also utilized this device to filter out the carrier and the negative sideband of an Electro-Optic Modulator (EOM) for the demonstration of a fast spatial light modulator³⁸. For yet-more-stable performance, the two-mirror cavity could be replaced with a doubly-convex fused-silica etalon, with stress applied directly to the glass. Although we only described and demonstrated the second-order filter, the even ($2N$ th-order) high-order filters are naturally generalizable, as shown in the Appendix. Better background rejection can be achieved by a combination of higher-performance polarizing beamsplitters and better mode matching into the resonator. A narrower passband is achievable by simply making the resonator longer.

ACKNOWLEDGEMENTS

Z.L. acknowledges support from the Urbanek-Chodorow Fellowship. This work was supported by the Office of Naval Research (ONR) through Grant N000142512198.

AUTHOR CONTRIBUTIONS

Z.L., A.V.K., and X.W. built and performed the experiments and data analysis. Z.L., A.V.K., and J.S. wrote the manuscript with contributions and input from all authors. J.S. supervised this project. Z.L., A.V.K., and X.W. contributed equally.

COMPETING INTERESTS

J.S. acts as a consultant to and holds stock options from Atom Computing.

DATA AVAILABILITY

The data that support the findings of this study are available from the corresponding author upon reasonable request.

Appendix A: S-matrix approach for coupled cavity

Here we derive the transmission (2) using the S-matrix approach from the first principle.

The base of the following calculation is 2-dimensional, with the upper one being right propagating and the lower one being left propagating.

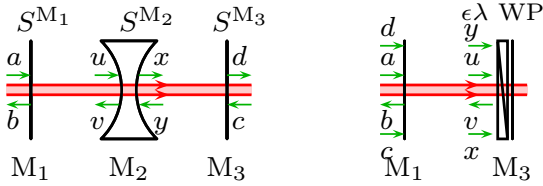


FIG. 5. S-matrix description of the two types of coupled cavity system.

Then, the scattering is given by

$$\begin{pmatrix} u \\ b \end{pmatrix} = S^{M_1} \begin{pmatrix} a \\ v \end{pmatrix}, \begin{pmatrix} x \\ v \end{pmatrix} = S^{M_2} \begin{pmatrix} u \\ y \end{pmatrix}, \begin{pmatrix} d \\ y \end{pmatrix} = S^{M_3} \begin{pmatrix} x \\ c \end{pmatrix}, \quad (A1)$$

where the fields are defined as in Fig. 5, and the scattering matrices are

$$\begin{aligned} S^{M_1} &= \begin{pmatrix} ie^{ikL_1}t_{M_1} & e^{2ikL_1}r_{M_1} \\ r_{M_1} & ie^{ikL_1}t_{M_1} \end{pmatrix}, \\ S^{M_2} &= \begin{pmatrix} it_{M_2} & r_{M_2} \\ r_{M_2} & it_{M_2} \end{pmatrix}, \\ S^{M_3} &= \begin{pmatrix} ie^{ikL_2}t_{M_3} & r_{M_3} \\ e^{2ikL_2}r_{M_3} & ie^{ikL_2}t_{M_3} \end{pmatrix}, \end{aligned} \quad (A2)$$

where r_{M_i}, t_{M_i} are the reflectivity and transmittivity coefficients of the three mirrors.

Each of the S-matrix can be converted into a T-matrix which can be calculated easily, as

$$T^{M_i} = \begin{pmatrix} S_{11}^{M_i} - S_{12}^{M_i}(S_{22}^{M_i})^{-1}S_{21}^{M_i} & S_{12}^{M_i}(S_{22}^{M_i})^{-1} \\ -(S_{22}^{M_i})^{-1}S_{21}^{M_i} & (S_{22}^{M_i})^{-1} \end{pmatrix},$$

and

$$\begin{pmatrix} d \\ c \end{pmatrix} = \underbrace{\mathbf{T}^{M_3} \mathbf{T}^{M_2} \mathbf{T}^{M_1}}_{\mathbf{T}^{\text{tot}}} \begin{pmatrix} a \\ b \end{pmatrix}, \quad (A3)$$

and at $c = 0$, the transmission T is

$$T = \left| \frac{d}{a} \right|^2 = \left| \mathbf{T}_{11}^{\text{tot}} - \frac{\mathbf{T}_{12}^{\text{tot}} \mathbf{T}_{21}^{\text{tot}}}{\mathbf{T}_{22}^{\text{tot}}} \right|^2. \quad (A4)$$

For simplicity, we let the two cavities be identical and the mirrors are lossless, i.e., $t_1 = t_3, r_1 = r_3, L_1 = L_3 = L, t_i^2 + r_i^2 = 1$. We also introduce the detuning δ of the laser from the resonance as in the main text, so that $e^{2ikL} = e^{i\delta/\text{FSR}}$, where $\text{FSR} = c/2L$. This simplifies the transmission to be

$$T = \frac{t_{M_1}^4 t_{M_2}^2}{A^2 + B^2},$$

where $A = (1 + r_{M_1}^2) \cos(2\pi\delta\nu/\text{FSR}) - 2r_{M_1}r_{M_2}$, and $B = t_{M_1}^2 \sin(2\pi\delta\nu/\text{FSR})$.

In the high finesse limit, $t_{M_1} \ll 1, t_{M_2} \ll 1$. We also expand the $\delta\nu$ to the 4-th order and we obtain

$$T \sim \frac{1}{\left(\frac{4r_{M_2}^2 + t_{M_1}^4}{4t_{M_1}^2 t_{M_2}} \right)^2 + \left(\frac{1}{2t_{M_2}^2} - \frac{2}{t_{M_1}^4} \right) \left(\frac{\delta}{\text{FSR}} \right)^2 + \frac{1}{t_{M_1}^4 t_{M_2}^2} \left(\frac{\delta}{\text{FSR}} \right)^4},$$

and is an ideal second order filter when $t_{M_2} = t_{M_1}^2/2$:

$$T \rightarrow \frac{1}{1 + \left(\frac{2\delta}{\text{FSR}t_{M_1}^2 \sqrt{2}} \right)^4}.$$

The intrinsic loss rate for both cavities (either formed by M_1, M_2 or M_2, M_3) is $\text{FSR}/\text{finesse}$, where the finesse is $1/t_{M_i}^2$. As the setup, the loss rate should be $\kappa/\sqrt{2}$, i.e., $\text{FSR}t_{M_1}^2 = \kappa/\sqrt{2}$. This leads to Eq. (2) as $T = 1/(1 + (2\delta/\kappa)^4)$.

Appendix B: 2D Density Plot

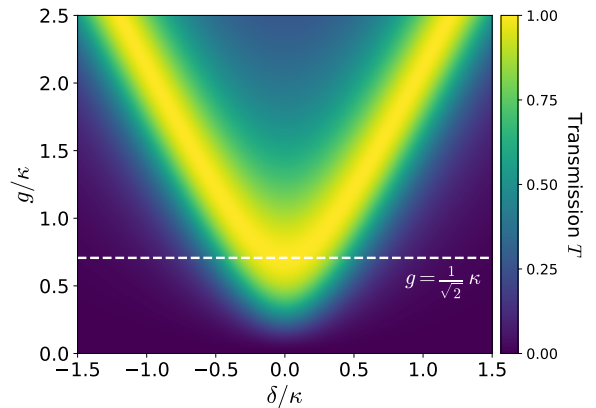


FIG. 6. Density plot of the simulated filtered spectrum. This plot depicts the form of the transmission as described by (5) as a function of the coupling strength g and the detuning from the center resonance of the filter δ . The white dashed line shows the critical coupling condition where $g = \kappa/\sqrt{2}$, where the transmission behaves as in (2).

Appendix C: Higher-order filter

The high-order Butterworth filters can be implemented by coupling multiple cavities at the same frequency, as shown in Fig. 7(a). The specific Hamiltonian is

$$\hat{H}_{\text{eff}} = \omega_c \mathbb{I}_n + \kappa \begin{bmatrix} i\frac{\gamma}{2} & J_1 & 0 & \dots & 0 \\ J_1 & 0 & J_2 & \dots & 0 \\ 0 & J_2 & 0 & \ddots & 0 \\ \vdots & \ddots & \ddots & \ddots & J_{N-1} \\ 0 & \dots & 0 & J_{N-1} & i\frac{\gamma}{2} \end{bmatrix}, \quad (C1)$$

where

$$\begin{aligned} J_i &= \frac{1}{4\sqrt{\sin\left[\frac{2i-1}{2N}\pi\right] \sin\left[\frac{2i+1}{2N}\pi\right]}}, \\ \gamma &= \frac{1}{2\sin\left[\frac{1}{2N}\pi\right]}, \end{aligned} \quad (C2)$$

where J_i are unitless tunneling rates between cavity i and $i+1$ normalized to the FWHM κ , and γ is the decay rate of the first

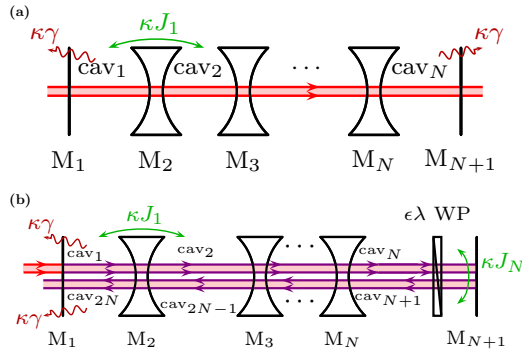


FIG. 7. Higher-order filter schemes (beams are drawn as a guide for the eye). (a) A general schematic for an N th-order filter with N coupled cavities. (b) A schematic for an even $2N$ th-order filter with N cavities. Each cavity has 2 polarization modes. Input light (red) is aligned to one of these polarization modes. These modes are coupled (violet) via a single intra-cavity birefringent optic to give coupled $2N$ cavity modes. The red curly arrows denote the loss of each cavity mode to the continuum and are denoted by $\kappa\gamma$. The green arrows represent the coupling between two cavity modes n and $n+1$ and are denoted by κJ_n .

and last cavity normalized to the FWHM κ . Practically, the coupling strength is determined by the mirror's transmission (assuming there is no loss)³⁹ (Ch. 12)

$$g_{i,i+1} = J_i \kappa = \sqrt{\text{FSR}_i \text{FSR}_{i+1} \cdot t_{M_{i+1}}}. \quad (\text{C3})$$

Specifically, the even-order filter can be efficiently implemented in the polarization basis, as shown in Fig. 7(b). Here, the coupling between cavity N and $N+1$ is introduced in the same way as in the main text through a tilted multi-order HWP or stressed glass plate, while the rest of the coupling is done by the mirrors' residual transmissions.

REFERENCES

- 1 R. L. Johnson, "Bandpass filters past and present," Tech. Rep. (Omega Optical Inc., 2016).
- 2 M. Technologies, "Quarter wave stack high reflection coatings, interference filters, and bandpass filters," Tech. Rep. (MPO Technologies, 2025).
- 3 R. L. Johnson, in *Optical Interference Coatings 2016* (Optica Publishing Group, 2016) p. TC.11.
- 4 H. J. Kimble, Y. Levin, A. B. Matsko, K. S. Thorne, and S. P. Vyatchanin, Phys. Rev. D **65**, 022002 (2001).
- 5 H. Levine, A. Keesling, A. Omran, H. Bernien, S. Schwartz, A. S. Zibrov, M. Endres, M. Greiner, V. Vuletić, and M. D. Lukin, Phys. Rev. Lett. **121**, 123603 (2018).
- 6 L. Li, W. Huie, N. Chen, B. DeMarco, and J. P. Covey, Phys. Rev. Appl. **18**, 064005 (2022).
- 7 J. Hald and V. Ruseva, J. Opt. Soc. Am. B **22**, 2338 (2005).
- 8 R. Fasano, Y. Chen, W. McGrew, W. Brand, R. Fox, and A. Ludlow, Phys. Rev. Appl. **15**, 044016 (2021).
- 9 N. Smith-Lefebvre, S. Ballmer, M. Evans, S. Waldman, K. Kawabe, V. Frolov, and N. Mavalvala, Opt. Lett. **36**, 4365 (2011).
- 10 M. Notcutt, L.-S. Ma, J. Ye, and J. L. Hall, Opt. Lett. **30**, 1815 (2005).
- 11 C. Fabre, R. G. DeVoe, and R. G. Brewer, Opt. Lett. **11**, 365 (1986).
- 12 T. Kessler, C. Hagemann, C. Grebing, T. Legero, U. Sterr, F. Riehle, M. J. Martin, L. Chen, and J. Ye, Nat. Photonics **6**, 687 (2012).
- 13 J. Alnis, A. Matveev, N. Kolachevsky, T. Udem, and T. W. Hänsch, Phys. Rev. A **77**, 053809 (2008).
- 14 X. Jiang, J. Scott, M. Friesen, and M. Saffman, Phys. Rev. A **107**, 042611 (2023).
- 15 T. Denecker, Y. T. Chew, O. Guillemant, G. Watanabe, T. Tomita, K. Ohmori, and S. de Léséleuc, Phys. Rev. A **111**, 042614 (2025).
- 16 D. P. Hoffman, D. Valley, S. R. Ellis, M. Creelman, and R. A. Mathies, Opt. Express **21**, 21685 (2013).
- 17 E. R. Lorenzo, B. Karki, K. E. White, K. H. Burns, and C. G. Elles, The Journal of Chemical Physics **161**, 224201 (2024).
- 18 Y. Amiel, R. Nedvedski, Y. Mandelbaum, Y. R. Tischler, and H. Tischler, Spectrochimica Acta Part A: Molecular and Biomolecular Spectroscopy **325**, 125038 (2025).
- 19 H. Levine, D. Bluvstein, A. Keesling, T. T. Wang, S. Ebadi, G. Semeghini, A. Omran, M. Greiner, V. Vuletić, and M. D. Lukin, Phys. Rev. A **105**, 032618 (2022).
- 20 A. Lagutchev, S. A. Hambir, and D. D. Dlott, The Journal of Physical Chemistry C **111**, 13645 (2007).
- 21 I. V. Stiopkin, H. D. Jayathilake, C. Weeraman, and A. V. Benderskii, The Journal of Chemical Physics **132**, 234503 (2010).
- 22 P. Hamm, M. Lim, and R. M. Hochstrasser, The Journal of Physical Chemistry B **102**, 6123 (1998).
- 23 D. M. Jonas, Annual Review of Physical Chemistry **54**, 425 (2003).
- 24 Z. Chen, X. Zhou, C. A. Werley, and K. A. Nelson, Applied Physics Letters **99**, 071102 (2011).
- 25 Q. Lin, M. A. V. Camp, H. Zhang, B. Jelenković, and V. Vuletić, Opt. Lett. **37**, 1989 (2012).
- 26 S. Butterworth, Wireless Engineer **7**, 536 (1930).
- 27 J. Scheuer and M. Shahriar, Optics letters **38**, 3534 (2013).
- 28 X.-B. Xu, X. Guo, W. Chen, H. X. Tang, C.-H. Dong, G.-C. Guo, and C.-L. Zou, Phys. Rev. A **100**, 023809 (2019).
- 29 N. Habler and J. Scheuer, Phys. Rev. A **101**, 043828 (2020).
- 30 H. Van de Stadt and J. M. Muller, Journal of the Optical Society of America A **2**, 1363 (1985).
- 31 X. Zhang, M. Singh, D. Li, and M. A. Popović, Opt. Lett. **49**, 3678 (2024).
- 32 M. Stone, A. Suleymanzade, L. Taneja, D. I. Schuster, and J. Simon, Optics Letters **46**, 21 (2020).
- 33 O. Naaman and J. Aumentado, PRX Quantum **3**, 020201 (2022).
- 34 G. L. Matthaei, L. Young, and E. M. T. Jones, *Microwave filters, impedance-matching networks, and coupling structures* (University Science Books, 1980).

³⁵H. Yan, X. Wu, A. Lingenfelter, Y. J. Joshi, G. Andersson, C. R. Conner, M.-H. Chou, J. Grebel, J. M. Miller, R. G. Povey, *et al.*, Applied Physics Letters **123** (2023), 10.1063/5.0161893.

³⁶J. Simon, *Cavity QED with atomic ensembles*, Ph.D. thesis, Harvard University (2010).

³⁷C. Cohen-Tannoudji, J. Dupont-Roc, and G. Grynberg, *Atom-Photon Interactions: Basic Processes and Applications* (John Wiley & Sons, 1998).

³⁸X. Wei, Z. Li, A. V. Karve, A. L. Shaw, D. I. Schuster, and J. Simon, “A 10 megahertz spatial light modulator,” (2026), arXiv:2601.08906 [quant-ph].

³⁹D. A. Steck, “Quantum and atom optics,” (2007).